

StormMind

AI based Web-Service for Storm Damage Prediction

Bachelor Thesis

ZHAW School of Engineering
Institute of Computer Science



Submitted on:

06.06.2025

Authors:

Gämperli Nils

Ueltschi Damian

Supervisor:

Andreas Meier

Study Program:

Computer Science



Declaration of Authorship

We, Damian UELTSCHI, Nils GÄMPERLI, declare that this thesis titled, “StormMind - AI based Web-Service for Storm Damage Prediction” and the work presented in it are our own. We confirm that:

- All external help, aids and the adoption of texts, illustrations and programs from other sources are properly referenced in the work.
- This is also a binding declaration that the present work does not contain any plagiarism, i.e. no parts that have been taken over in part or in full from another’s text or work under pretence of one’s own authorship or without reference to the source.
- In the event of misconduct of any kind, Sections 39 and 40 (Dishonesty and Procedure in the Event of Dishonesty) of the ZHAW Examination Regulations and the provisions of the Disciplinary Measures of the University Regulations shall come into force.

I have no limitations.
— Thomas Shelby

To our parents...

Abstract

Extreme weather events cause considerable damage to infrastructure, the economy and the environment worldwide. Predicting such damage can help to optimize preventive measures and reduce costs. In this project, a neural network is being developed that analyzes historical weather data and damage reports to predict potential storm damage in Switzerland based on new weather forecasts. Using modern machine learning techniques, relevant patterns are recognized in order to train a predictive model. The model is tested for accuracy and optimized to enable reliable predictions.

Key words: Machine Learning, Neural Network, Storm Damages



Acknowledgements

We would like to thank Andreas Meier for his valuable support and guidance throughout this project. Additionally, we would like to thank to Dr. Katharina Liechti which has provided us with valuable insights about the sciences of weather and storm damages. For providing and collecting data to make this project possible, we also like to thank to the Swiss Federal Institute for Forest, Snow and Landscape Research WSL.

Preface

Lorem ipsum dolor sit amet, consectetur adipiscing elit, sed do eiusmod tempor incididunt ut labore et dolore magnam aliquam quaerat voluptatem. Ut enim aequale doleamus animo, cum corpore dolemus, fieri tamen permagna accessio potest, si aliquod aeternum et infinitum impendere malum nobis opinemur. Quod idem licet transferre in voluptatem, ut postea variari voluptas distinguere possit, augeri amplificarique non possit. At etiam Athenis, ut e patre audiebam facete et urbane Stoicos irridente, statua est in quo a nobis philosophia defensa et collaudata est, cum id, quod maxime placeat, facere possimus, omnis voluptas assumenda est, omnis dolor repellendus. Temporibus autem quibusdam et.

Lorem ipsum dolor sit amet, consectetur adipiscing elit, sed do eiusmod tempor incididunt ut labore et dolore magnam aliquam quaerat voluptatem. Ut enim aequale doleamus animo, cum corpore dolemus, fieri tamen permagna accessio potest, si aliquod aeternum et infinitum impendere malum nobis opinemur. Quod idem licet transferre in voluptatem, ut.

Key words:

Contents

Declaration of Authorship	ii
Abstract	i
Acknowledgements	ii
Preface	iii
Contents	i
List of Abbreviations	iii
1 Introduction	1
1.1 Motivation	1
1.2 Work Outline	1
2 Theoretical Background	2
2.1 Weather Research	2
2.1.1 Reason for Flooding	3
2.1.2 Reason for Landslide	4
2.2 Deep Learning	4
2.2.1 Feedforward Neural Networks	4
2.2.2 The Backpropagation Training Algorithm	6
2.2.3 Recurrent Neural Networks	7
2.2.4 Long Short Term Memory Neural Networks	8
2.2.5 Transformer	10
2.3 Software Engineering	13
3 Methodology	14
3.1 Data	14
3.1.1 Data Cleaning	15
3.1.2 Availability of Sources and Data Collection	15
3.1.3 Data Preparation	16

3.2	Deep Learning Experiments	19
3.2.0.1	(?? FNN ??)	20
3.2.0.2	(?? LSTM ??)	21
3.2.1	Transformer	21
3.3	Software Engineering	22
3.3.1	Backend	22
3.3.1.1	Technologies	22
3.3.1.2	Architecture	22
3.3.2	Frontend	22
3.3.2.1	Technologies	22
3.3.3	Test Concept	22
4	Results	23
4.1	Results of AI Engineering	23
4.1.1	Feedforward Neural Network: Results	23
4.1.2	LSTM Neural Network	24
4.2	Combined	24
4.3	Conclusion	24
4.4	Software Results	25
5	Discussion and Outlook	26
	Bibliography	27
	List of Figures	30
	List of Tables	32
A	Appendix	33
AA	Disclaimer	33
AB	Original Data Features	34

List of Abbreviations

FNN	Feedforward Neural Network	RNN	Recurrent Neural Network
LSTM	Long Short Term Memory Neural Network	VGP	Vanishing Gradient Problem
NN	Neural Network	WSL	Swiss Federal Institute for Forest Snow and Landscape Research WSL

1 Introduction

1.1 Motivation

Why do we do this?

1.2 Work Outline

What do we want to predict etc.

2 Theoretical Background

This chapter presents the theoretical foundations required to understand the methods and models used in this work. The first part provides an overview of the physical and environmental aspects relevant to the prediction of storm-induced damage, including the meteorological mechanisms behind severe weather events and their typical impact patterns. This domain knowledge is essential for identifying meaningful input features and understanding the context of the prediction task.

The second part introduces the machine learning and deep learning concepts that underpin the modeling approach. It starts with basic Feedforward Neural Network (FNN) and progresses toward more advanced architectures tailored for sequential data, such as Recurrent Neural Network (RNN), Long Short Term Memory Neural Network (LSTM), and Transformer models. These architectures form the core of the predictive models developed in this thesis.

By combining insights from both atmospheric science and data-driven modeling, this chapter establishes the conceptual framework for the design and implementation of the storm damage forecasting pipeline.

2.1 Weather Research

The causes mentioned in this section are neither exhaustive nor account for all damages listed in [1]. In a conversation with K. Liechti ([2]), several contributing factors were discussed, of which only a subset were considered in the model. The discussed influencing factors were:

Topological gradients: The question addressed was whether known threshold values of slope (in percent or degrees) exist to differentiate between low, intermediate, and high landslide risk. Unfortunately, the answer was negative. Due to time constraints during the thesis project, further research — e.g., literature reviews — could not provide any conclusive information.

Forest/Deforestation: According to Wikipedia ([3]), deforestation contributes to landslides by eliminating trees, thereby destroying the stabilizing effect of their roots. K. Liechti confirmed this statement but also pointed out that forests themselves possess considerable weight, which may also contribute to slope instability. Applying this insight would require additional data and investigation, and was therefore deprioritized due to time limitations.

Soil condition: This factor is discussed in detail within each relevant subsection.

Ground frost: Frozen soil exhibits increased cohesive strength, which helps prevent landslides.

Rainfall: Closely linked to soil conditions; specifically addressed in each subsection.

Snowfall: Snowfall itself does not directly cause the damages under investigation but serves as a source for later snowmelt.

Snowmelt: Significantly contributes to the total volume of water input and has effects comparable to rainfall.

Small animals and soil organisms: This topic lies outside the scope of K. Liechti's expertise and was excluded from further consideration due to limited time.

2.1.1 Reason for Flooding

Flooding is primarily mitigated by the soil's capacity to absorb water. The composition of the topsoil is the most relevant factor: a non-permeable surface—such as rock or compacted clay—prevents infiltration, resulting in all incoming water contributing to surface runoff. In contrast, permeable materials such as sand or loose soil can absorb substantial amounts of water, depending on the depth of the soil layer (further details in Section 2.1.2). Even permeable ground can temporarily become impermeable during early spring when frozen. At the opposite extreme, drought has a similar effect: extended periods of high temperature and absent precipitation dry out the surface layer of the soil, thereby reducing or even eliminating its ability to absorb water. The behavior of completely dry soil is comparable to that of any other non-permeable material. All of these mechanisms are governed by the total water input, which originates either from rainfall, melting snow, or temperature conditions [2].

Prolonged precipitation continuously supplies water to the soil. If the ground is permeable and allows both infiltration and subsurface drainage, the overall impact remains limited. However, when the absorbed water cannot drain away, saturation occurs. Once the soil reaches full capacity, it effectively becomes impermeable—regardless of its natural permeability—and behaves like rock or clay, leading to increased surface runoff. In addition, sudden and sustained temperature increases—often indicative of significant snowmelt—can further augment the water load on the soil surface alongside rainfall. [2]

2.1.2 Reason for Landslide

Of the potential causes for landslides, three were considered. The first—loose gravel or rock—is not directly influenced by current weather conditions and was therefore excluded. The second and relevant factor is the water absorption capacity of loose soil (e.g., dirt). As water is absorbed, the soil mass increases in weight—from dry ($0.83\text{kg}/\text{dm}^3$ [4]) to wet ($1.6 - 1.76\text{kg}/\text{dm}^3$ [5]). This gain in mass reduces the soil's ability to remain stable. Additionally, subsurface clay layers limit water infiltration on the one hand, but on the other hand, they promote landslides by forming smooth and slippery interfaces between different soil types and by preventing subsurface drainage. In contrast, a jagged and solid rock surface also impedes subsurface drainage but may reduce landslide risk by mechanically anchoring the overlying soil layer. [2]

2.2 Deep Learning

Deep Learning has gained increasing popularity in recent years, particularly through advancements in Neural Networks (NNs). These developments have significantly expanded the capabilities of automated data-driven modeling across various domains. In this chapter, we focus primarily on NNs architectures, as they form the core modeling approach used in this project.

2.2.1 Feedforward Neural Networks

Feedforward Neural Networks (FNNs) are a class of machine learning models inspired by the structure and function of the human brain. In biological systems, neurons are interconnected through synapses, and their strengths change in response to external stimuli—a process that underlies learning. FNNs mimic this behavior by using computational units, also called neurons, connected by weighted links. These weights are adjusted during training to improve the model's predictions, analogous to synaptic strength adjustments in the brain.

Each artificial neuron receives inputs, scales them using learned weights, applies a non-linear activation function, and forwards the result to subsequent neurons. Through this architecture, an FNN models complex functions by propagating signals from input to output layers. Learning in FNNs occurs via exposure to training data consisting of input-output pairs. The network adjusts its weights to reduce the difference between its predictions and the target outputs, thereby minimizing the prediction error.

While the biological analogy is imperfect, it has historically guided the development of neural architectures. More formally, FNNs can also be viewed as compositions of simple mathematical units—such as logistic or linear regressors—structured into a computational graph. Their

expressive power arises from stacking these units into deeper networks, enabling them to approximate highly non-linear relationships in data. This capacity to learn from examples and generalize to unseen inputs makes FNNs a powerful tool in modern machine learning.

Architecture

An FNN trained with backpropagation, which is discussed in Section 2.2.2, can be illustrated as a directed acyclic Graph with inter-connections. It contains a set of neurons distributed in different layers.

- Each neuron has a activation function.
- The first layer, shown on the left side in Figure 2.1, is called the input layer and has no predecessors in the inter-connection graph. Additionally, is their input value the same as their output value.
- The last layer, shown on the right side in Figure 2.1, is called the output layer and have no successors in the inter-connection graph. Their value represents the output of the Network
- All other neurons are grouped in the so called hidden layers. In Figure 2.1 this is represented by the layer in the middle. A neural network can have an arbitrary amount of hidden layers.
- The edges in the inter-connection graph, are so called weights, which represent an arbitrary number in \mathbb{R} . These weights are updated during the trianing process.

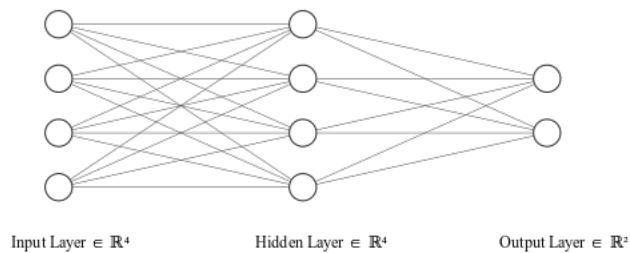


Figure 2.1 – Illustration of a Neural Network with 3 layers. Illustrated with [6]

Computation of the Output

The calculation of the output of the FNN is also called a forward pass. To do so, the value of each neuron needs to be calculated. This is done by summing all the inputs and then put this value into a given activation function. Mathematically, this process can be represented as: $y = f\left(\sum_i^n \xi_i\right)$ wher f represents the activation function of the neuron and ξ_i the input or also called the potential of a neuron. To compute a full forward pass, this is done for each neuron from the input layer towards the output layer. When a value is passed throughtouh a weight to a successor neuron, the value is multiplied by the value of the weight. This process can then be summarized to:

$$\begin{aligned}
y_1 &= f\left(\sum_i^n w_{ij}x_i\right) \text{ [input to hidden layer]} \\
y_{j+1} &= f\left(\sum_i^n w_{ij}y_j\right) \forall j \in \{1 \dots k-1\} \text{ [hidden to hidden layer]} \\
o &= f(w_{ij+1}y_j) \text{ [hidden to output layer]}
\end{aligned} \tag{2.1}$$

[7] where j denotes the layer, ascending from input layer to output layer, f activation function, w_{ij} weight at index i and layer j , x as input at index i . The state of the neuron in the output layer o can then be denoted as the output vector.

2.2.2 The Backpropagation Training Algorithm

Objective: To identify a set of weights that guarantees that for every input vector, the output vector generated by the network is identical to (or sufficiently close to) the desired output vector.

Note: The actual or desired output values of the hidden neurons are not explicitly specified by the task.

For a fixed and finite training set: The objective function represents the total error between the desired and actual outputs of all the output neurons for all the training patterns.

Error Function

$$E = \frac{1}{2} \sum_p^P \sum_i^N (y_{ip} - d_{ip})^2 \tag{2.2}$$

[8]

where P is the number of training patterns, N the number of output neurons, d_{ip} is the desired output for pattern p , y_{ip} the actual output of the neuron i and output neuron i .

Procedure

1. Compute the actual output for the presented pattern
2. Compare the actual output with the desired output
3. Adjustment of weights and thresholds against the gradient of the error function (Equation (2.2)) for each layer from the output layer towards the input layer

Figure 2.2 – Training Procedure of the backpropagation algorithm

Adjustment Rules

$$\begin{aligned}
w_{ij}(t+1) &= w_{ij} + \Delta_E w_{ij}(t) \\
\Delta_E w_{ij} &= -\frac{\partial E}{\partial w_{ij}} = -\frac{\partial E}{\partial y_j} \frac{\partial y_j}{\partial \xi_j} \frac{\partial \xi_j}{\partial w_{ij}}
\end{aligned} \tag{2.3}$$

[8]

where $\Delta_E w_{ij}$ denotes the change of the Error Function with respect to w_{ij} , E the Error Function, y_j the output of the output neuron j , ξ_j the potential of the neuron j and w_{ij} the weight with index i at layer j .

2.2.3 Recurrent Neural Networks

The feedforward FNNs discussed in Section 2.2.1 are inherently limited to fixed-size, unordered input representations. This makes them unsuitable for sequential data, where both the order and length of the input can vary. To address this limitation, we introduce a class of models specifically designed to process variable-length sequences: **RNNs**

Architecture

A **RNN** consists of the following components:

- **Input signal:** The external data which is fed into the network at a timestep n and represent the current information which the network is processing.
- **State signal:** Also known as the hidden state, represents the memory of the **RNN** for a given neuron. It contains information about the past inputs in the sequence and is updated at each time step based on the current input and the previous state. The hidden state is updated with the following formula: $h_t = f(h_{t-1}, x_t)$. After the update, the hidden state of neuron i serves as input into the neuron $i + 1$
- **Weights:** The weights of the **RNN** neurons are shared among all different states.
- **Output:** Each neuron has a output, which is denoted as $y_1 - y_4$ in Figure 2.4. This output can serve as the output for the current state or as input into the next neuron.

[9], [7]

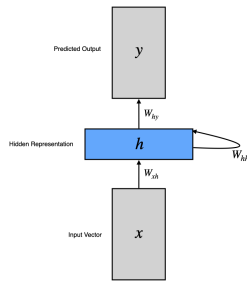


Figure 2.3 – RNN

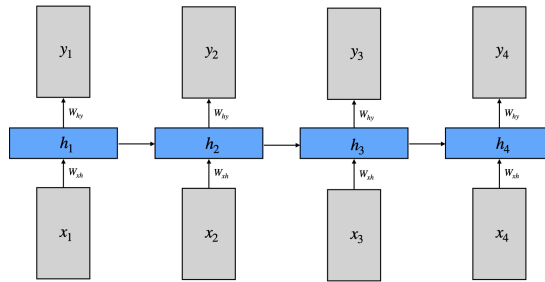


Figure 2.4 – 4 times unrolled RNN

Vanishing Gradient Problem

The Vanishing Gradient Problem (VGP) is a challenge encountered during the training of RNNs, particularly dealing with deep RNNs and long input sequences. It arises from the way how gradients are updated during the backpropagation algorithm (discussed in Section 2.2.2), which updates the network's parameters / weights by propagating gradients backward through each time step. In backpropagation, gradients are computed via the chain rule, resulting in repeated multiplication of weight matrices and derivatives of activation functions across time steps. When these values are consistently smaller than one, the gradients exponentially decrease as they traverse earlier layers or time steps. Consequently, the gradients become vanishingly small, leading to negligible updates for earlier parameters and impairing the network's ability to learn long-range dependencies. The same principle arises, when the gradients become too large. In this case, the problem is called the exploding gradient problem.

[7]

2.2.4 Long Short Term Memory Neural Networks

Long Short Term Memory Neural Networks (LSTMs) are a special form of RNNs designed to address the problem of Vanishing Gradients while having a more fine-grained control over the previous input data and were introduced for the first time by Sepp Hochreiter in 1997 [10]. LSTMs are an enhancement of RNNs, because the recurrence conditions of how the hidden state h_t is processed. To achieve this aim, we introduce a new hidden state of the same dimension as h_t , which is called the cell state and is denoted as c_t . The key innovation of the LSTM lies in its ability to control the flow of information using a set of gating mechanisms. These gates regulate how information is added to, removed from, or exposed from the cell

state. Each gate is implemented as a sigmoid-activated neural layer and serves a distinct role in the update process.

Architecture

The internal structure of an **LSTM** cell is shown in Figure 2.5. The figure illustrates how, at each time step t , the cell takes in the input vector x_t , the previous hidden state h_{t-1} , and the previous cell state c_{t-1} , and uses them to compute updated values for the current cell state c_t and hidden state h_t .

Figure 2.5 shows an illustration of an **LSTM** Cell.

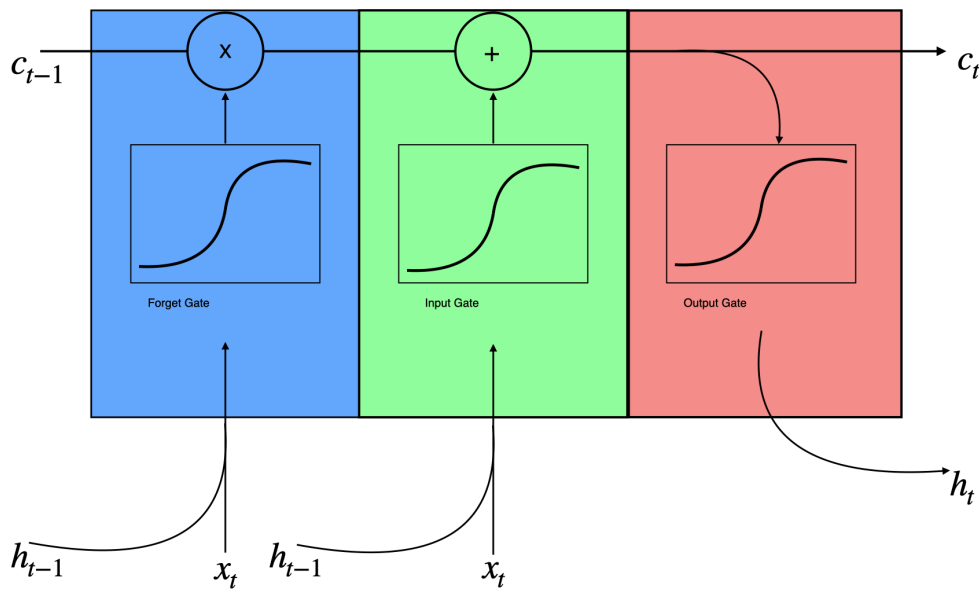


Figure 2.5 – Schematic illustration of an **LSTM** cell highlighting the internal gating structure. The colored blocks represent the three core gates—Forget (blue), Input (green), and Output (red)—and show how they interact with the cell and hidden states to regulate information flow.

At each time step t with a given input vector x_t , previous hidden state h_{t-1} and previous cell state c_{t-1} , the **LSTM** performs the following computations:

- Forget Gate (shown in the blue part of Figure 2.5): This gate decides which parts of the previous cell state should be forgotten. The value of the forget gate is calculated as:
 - $f_t = \sigma(w_f[h_{t-1}, x_t]) + b_f$
- Input Gate (shown in the green part of Figure 2.5): Decides which new information will be added to the cell state and is calculated as:
 - $i_t = \sigma(w_i[h_{t-1}, x_t] + b_i)$

- Output Gate (shown as the red part in Figure 2.5): Determines which part of the cell state influences the hidden state and therefore the output. It is computed with:
 - $o_t = \sigma(w_o[h_{t-1}, x_t] + b_o)$
- Candidate Cell State: Computes possible candidates \tilde{c}_t which can be added to the cell state, computed as:
 - $\tilde{c}_t = \tanh(w_c[h_{t-1}, x_t] + b_c)$
- Cell state update: Given the candidates, the cell state can be updated as:
 - $c_t = f_t \cdot c_{t-1} + i_t \cdot \tilde{c}_t$
- Hidden state update: The final hidden state is computed by applying the output gate to the activated cell state. It is computed with:
 - $h_t = o_t \cdot \tanh(c_t)$

Note: w_x represents a complete weight matrix for each gate, b_x denotes the bias for the corresponding gates, and σ denotes the sigmoid function.

[11], [12]

2.2.5 Transformer

With the advent of Large Language Models and influential works such as Attention Is All You Need [13], Transformer architectures have gained significant traction in the field of machine learning. Originally developed for natural language processing tasks, Transformers have since been successfully adapted to a variety of domains, such as time series forecasting as shown by Q. Wen et. al. in “Transformers in Time Series: A Survey” [14] due to their ability to model long-range dependencies.

In the following section, the core components and mechanisms of the Transformer architecture are outlined. Furthermore, special emphasis is placed on its applicability to time series forecasting—a setting in which capturing temporal patterns and complex dependencies is crucial.

Architecture

An important concept in the Transformer architecture is Attention. It allows the model to capture dependencies between elements in the input sequence. An attention function can be viewed as a mapping from a query and a set of key–value pairs to an output. The output is a weighted sum of the values, where the weights are determined by a compatibility function between the query and the keys. This mechanism is illustrated in Figure 2.6, where the input sequence is linearly projected into query, key, and value matrices to compute attention scores and generate contextualized representations. In tasks involving sequential data, such as language modeling or time series forecasting, the model should not have access to future positions when making a prediction. To enforce this constraint, the Transformer uses a

technique called masked attention, in which the attention weights for all positions beyond the current one are set to zero. This ensures that, when computing the representation for position x_n , the model can only attend to $x_{<n}$ through x_n , but not to any $x_{>n}$.

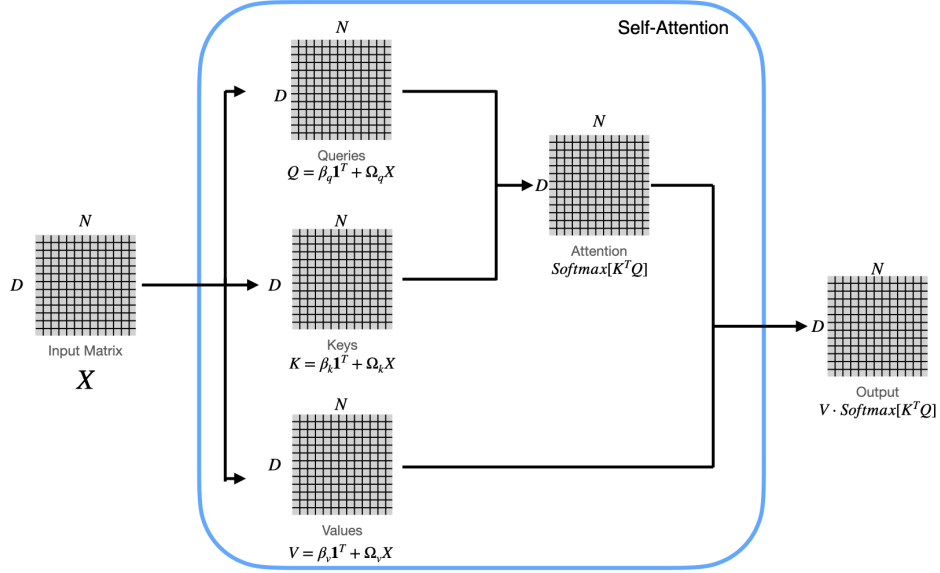


Figure 2.6 – Self-attention mechanism illustrated with matrices. All matrices have shape $D \cdot N$, where D is the sequence length and N is the feature dimension. The input matrix is projected into three separate matrices: Queries (Q), Keys (K), and Values (V). The attention weights are computed by multiplying Q with the transpose of K , followed by the Softmax function. The result is then used to weight the V matrix, producing the final output as $\text{Softmax}(QK^T) \cdot V$. [15]

[13], [16], [15]

Transformers follow an encoder-decoder architecture, as illustrated in Figure 2.7. In this framework, the encoder processes the full input sequence and produces a contextual representation, called the Encoder Vector as shown in Figure 2.7 in grey. The decoder uses the Encoder Vector to generate the output sequence token by token. While both encoder and decoder are composed of multiple stacked layers and share a similar modular structure, including feedforward sub-layers, skip connections, and normalization steps. The decoder includes additional mechanisms to ensure autoregressive generation, which refers to the process of generating output tokens one at a time and each token is generated based on all previous generated tokens.

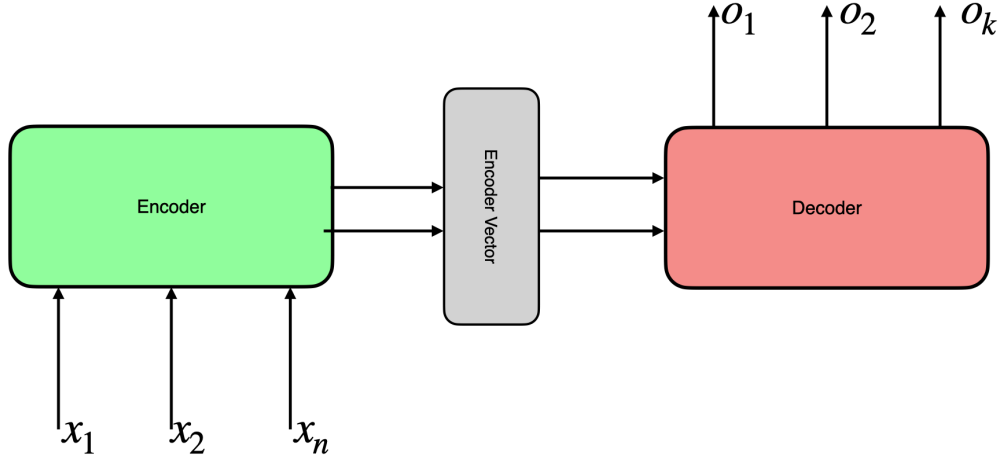


Figure 2.7 – Abstracted illustration of the encoder–decoder architecture. The encoder receives an input sequence x_1, \dots, x_n and transforms it into a sequence of contextualized representations, here called the Encoder Vector, which is symbolically represented by two arrows to emphasize its role in guiding the decoding process. The encoder vector are passed to the decoder, which generates an output sequence y_1, \dots, y_k , where the output length k may differ from the input length n . [7]

Combining the encoder–decoder structure with the attention mechanism results in the full Transformer model. In this architecture, self-attention is used within both the encoder and decoder to enable each position in a sequence to access contextual information from all other positions.

During training, the encoder receives the full observed input sequence, such as past weather patterns over several weeks in the domain of weather forecasting. The decoder is provided with the leftmost portion of the target sequence, which is, the known values from the beginning of the forecast window. For example, if the goal is to predict the temperature over the next 10 days, the decoder might initially receive only a start-of-sequence token or the first known value and must predict the next value in the sequence. To prevent the decoder from accessing future values during training, a masking strategy is applied in the self-attention, layers. This ensures that each prediction depends only on earlier positions in the output sequence, simulating real-world forecasting conditions. The model is trained by comparing each predicted value to the actual value using a suitable loss function such as cross-entropy or mean squared error, depending on the output type. This approach enables the model to learn autoregressive

generation, where each future value is predicted step by step, conditioned on both the encoder input and previously predicted outputs. [7]

Although the original Transformer combines encoder and decoder modules, simplified variants such as BERT and GPT-3 omit either the decoder or encoder component. BERT uses an encoder-only architecture suited for classification and representation tasks, while GPT-3 is built on a decoder-only architecture optimized for generative tasks. [16]

2.3 Software Engineering

3 Methodology

3.1 Data

The basis of the data was provided by the Swiss Federal Institute for Forest Snow and Landscape Research WSL (WSL). The correspondence partner was K. Liechti, who provided valuable insights into the data as well as into the relevant geographical and meteorological processes. To comply with the legal restrictions cited in Appendix AA, the use of WSLs data in this thesis was limited. These limitations ultimately proved beneficial to the modeling process, as demonstrated by the experiments.

The sources for the recorded incidents were Swiss newspapers. As a result, the accuracy of the incident locations cannot be guaranteed, and the (financial) extent of the damages is only an approximation. In some cases, the location could not be precisely determined; thus, only the region or canton was recorded. Due to these uncertainties, the financial extent had to be rounded, and the damages grouped by canton or region prior to publication.

As outlined in Appendix AB, the scope of the dataset was extensive. The features selected for this thesis were limited to the following: “Gemeindenamen”, “Datum”, “Hauptprozess”, and “Schadensausmass”, which were identified as the most relevant variables related to damage.

Based on the inputs of K. Liechti, the relevant meteorological variables were identified as sunshine duration, ground temperature, snowfall, and rainfall.

The rationale for this selection is briefly summarized below; detailed explanations can be found in Section 2.1:

Sunshine hours influence ground temperature, which in turn can cause snowmelt or thaw ground frost.

Ground temperature was not available via open-meteo[17]; therefore, the temperature at 2 meters above ground was used as a proxy.

Snowfall can contribute to snowmelt processes later in the seasonal cycle.

Rainfall directly contributes to the potential for flooding and can also indirectly increase ground temperature.

In a subsequent experiment, snowfall was found to have no significant impact and was therefore completely removed from the dataset.

3.1.1 Data Cleaning

The damage data referenced in Section 3.1 required several processing steps before it could be used in the modeling phase. As noted in Appendix AA, the municipality names correspond to the administrative boundaries of 1996 and are thus not up to date. To identify outdated names, GPS coordinates were retrieved using the Geocoding API [18]. For approximately 300 out of 2759 municipalities, no coordinates could be retrieved. Manual analysis of these cases revealed recurring issues.

For some incidents, as described in Section 3.1, WSL could not determine the exact location and had to assign them to a canton (30 of 28,515 cases), region (3), or district (10). Due to their low frequency, these entries were excluded from the dataset.

Common abbreviations used in the WSLs dataset—such as “a.A.” for “am Albis” or “St.” for “Sankt”—were standardized. Additionally, some municipalities had been merged into others since 1996. These cases were manually updated with their current names.

The weather data required less preprocessing. In eight municipalities, occasional values were set to ‘null’ (no data available); these were replaced by 0.

3.1.2 Availability of Sources and Data Collection

The data currently in use was collected with relatively little difficulty. The damage data was kindly provided by K. Liechti from the WSL following a formal request via email [19].

For the collection of weather data, the initial approach was to use official government data provided by MeteoSwiss [20]. However, due to the structure of the website and the raw nature of the station-based measurement data, this approach was ultimately abandoned. During further research, the open-meteo API [17] was discovered. To avoid excessive costs, a free academic access key was requested and kindly provided [21].

To obtain information on soil conditions, the first resource consulted was the Swiss federal geoportal map.geo.admin [22]. However, the format of the data was mostly incompatible with the tools available for this thesis. An alternative considered was the GIS Browser [23], which is the cantonal equivalent of map.geo.admin [22]. Unfortunately, it posed the same limitations as the federal source.

Given that new buildings are constantly being constructed in Switzerland and that the Swiss Confederation is actively researching locations for a nuclear waste repository [24], it was assumed that public institutions must maintain relevant geotechnical data.

First, the building construction office of Affoltern am Albis was contacted [25]. They referred the inquiry to the cantonal building construction office, which also denied possession of such data and redirected the request to the Office for Spatial Development [26].

The contact person from the Office for Spatial Development [27] was likewise unable to provide relevant data or further contacts. Their suggestion was to consult the GIS Browser [23] or map.geo.admin [22].

After these repeated unsuccessful attempts, the GIS Helpdesk was contacted [28]. The proposed solution [29] was again to use the GIS Browser or map.geo.admin, which had already proven inadequate. Due to time constraints, this approach was ultimately abandoned.

3.1.3 Data Preparation

After collecting all relevant datasets, a series of preprocessing steps were applied to construct a complete spatio-temporal dataset suitable for storm damage forecasting.

Adding Non-damage Data:

The original dataset, discussed in Section 3.1 provided by WSL contained only records of storm damage events, each described by the attributes: Date, Municipality, Main Process, and Extent of Damage. However, to train a forecasting model, it was necessary to include days and locations with no reported damage. Therefore, the dataset was extended by computing the Cartesian product of:

$$\text{Dates} \times \text{Municipalities} \quad (3.4)$$

Let D denote the set of all the dates from 1972 to 2023 and M the set of all Swiss municipalities based on the Swiss official commune register [30] published in 2013. We constructed:

$$X = \{(d, m)\} \mid d \in D, m \in M \quad (3.5)$$

This set was then left-joined with the original storm damage records. For entries where no damage was reported, the fields Extent of Damage and Main Process were imputed with zeros. Furthermore, due to political changes over the decades (e.g., municipal mergers), all historical municipality names were mapped to their most recent equivalent, based on the Swiss official commune register [30]. As a result, the final base dataset consisted of 52,399,36 rows of which:

- 52'372'088 represented non-damage instances
- 24'613 corresponded to small damage events
- 1'800 were classified as medium damage

- 859 indicated large-scale damages

Spatial Clustering:

To address the extreme class imbalance and to comply with WSLs data usage disclaimer (Appendix AA), we aggregated municipalities into k spatial clusters using k-means clustering on geographic coordinates (latitude and longitude). Let $x_i = (\lambda_i, \varphi_i)$ be the coordinates for municipality i . The clustering objective was to minimize:

$$\sum_{i=1}^N \min_{j \in \{1 \dots k\}} (\|x_i - \mu_j\|)^2 \quad (3.6)$$

[31] where μ_j denotes the centroid of cluster j . This was implemented using the KMeans algorithm from SciKitLearn [32].

To ensure deterministic behavior of the KMeans algorithm from SciKitLearn [32], we specified both the `random_state` parameter and a fixed number of initializations. In particular, we set: `random_state= 42` and `n_init = 10`. This guarantees that, for a given number of clusters k , the clustering results are identical across repeated runs. The `random_state` controls the random number generation used for centroid initialization, and setting it ensures reproducibility of the clustering outcome. [32]

Figure 3.8 presents an illustrative example of the spatial clustering of all municipalities into $k = 6$ clusters. The black crosses indicate the centroids of the respective clusters.

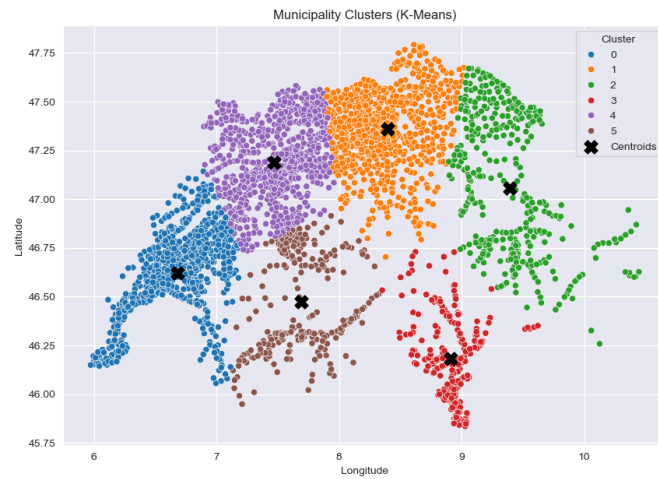


Figure 3.8 – Example clustering of all Swiss municipalities with $k = 6$

Each damage entry was then aggregated per cluster center and normalized by a weighted sum reflecting the severity of the damage class (small, medium, large). This yielded a dataset with k time series, one for each cluster.

Temporal Grouping:

The data were then aggregated at weekly intervals. For each cluster and week, the total storm damage was computed by summing the mean monetary value assigned to each damage class. Specifically, each daily damage event was replaced by the average monetary damage associated with its class (as derived from the original dataset). Then, the total weekly damage was calculated as:

$$\text{Damage}_{\text{week}} = \sum_{\text{day} \in \text{week}} \text{MeanDamage}_{\text{class}(\text{day})} \quad (3.7)$$

$\text{MeanDamage}_{\text{class}(\text{day})}$ is the average damage in CHF for the class of the damage event on that day. The averages were provided by K. Liechti (WSL):

- Class 1 (small): 0.06 Mio CHF
- Class 2 (medium): 0.8 Mio CHF
- Class 3 (large): 11.3 Mio CHF

The final dataset consists of entries with the following attributes per time window (week) and cluster center:

- end_date: last day of the week
- center_municipality: name of the cluster centroid
- cluster_center_latitude, cluster_center_longitude: Geographical coordinates of the cluster center
- damage_grouped: aggregated and binned damage label (0-3)

To convert the continuous aggregated damage values into categorical classes, we defined a binning procedure based on quantiles of the non-zero damage distribution.

Let $D = \{d_1, d_2, \dots, d_n\}$ be the set of non-zero aggregated damage values and q_1, q_2, q_3 be the proportions of the damage classes where $q_1 = 0.9005, q_2 = 0.0667, q_3 = 0.0328$. The bin thresholds T_{low} and T_{mid} were computed as:

$$\begin{aligned} T_{\text{low}} &= \text{percentile}(D, 100 * q_1) \\ T_{\text{mid}} &= \text{percentile}(D, 100 * (q_1 + q_2)) \end{aligned} \quad (3.8)$$

They also depend on the number of spatial clusters k , which determines how many data points contribute to the distribution of damages per region. Then, the aggregated damage values were classified into four ordinal classes based on the following thresholds:

- Class 0: ($d = 0$)
- Class 1: ($0, T_{\text{low}}$]
- Class 2: ($T_{\text{low}}, T_{\text{mid}}$]
- Class 3: (T_{mid}, ∞)

3.2 Deep Learning Experiments

The goal of the experiments was to identify the most suitable deep learning architecture for predicting storm damage events based on weather-related input features. We evaluated different types of neural networks, beginning with a baseline Feedforward Neural Network (FNN), and compared their performance on a held-out test set.

Datasets

As shown in Table 3.1 dataset was temporally split into training, validation, and test sets to simulate realistic forecasting scenarios and prevent information leakage. The training set spans the years 1971–2002, the validation set covers 2003–2013, and the test set includes data from 2013–2023.

Table 3.1 – Datasets splits

Set	Nr of patterns	Years
Train	10014	1971 - 2002
Validation	3132	2003 - 2013
Test	3132	2013 - 2023

Training Pipeline

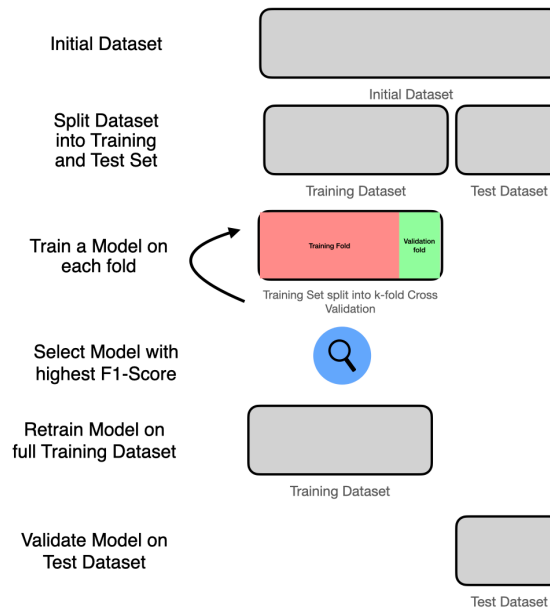


Figure 3.9 – Training Pipeline illustrated

3.2.0.1 Feedforward Neural Network (FNN)

Our first experiment employed a baseline Feedforward Neural Network (FNN), whose architecture is illustrated in Figure 3.10. The network consists of 10 fully connected layers with ReLU activation functions. The model was trained using the Adam optimizer and cross-entropy loss.

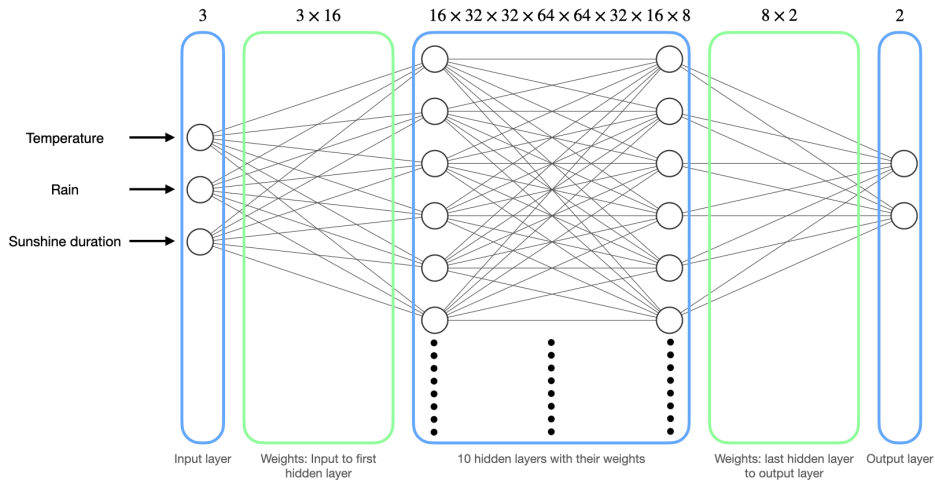


Figure 3.10 – Illustration of the used FNN

Input features

The input to the FNN consisted of three weather-related variables: mean temperature at 2 meters, total rainfall, and snow accumulation. All features were normalized to zero mean and unit variance, as described in Section 3.1, and were provided on a weekly basis for each coordinate in the dataset.

Training

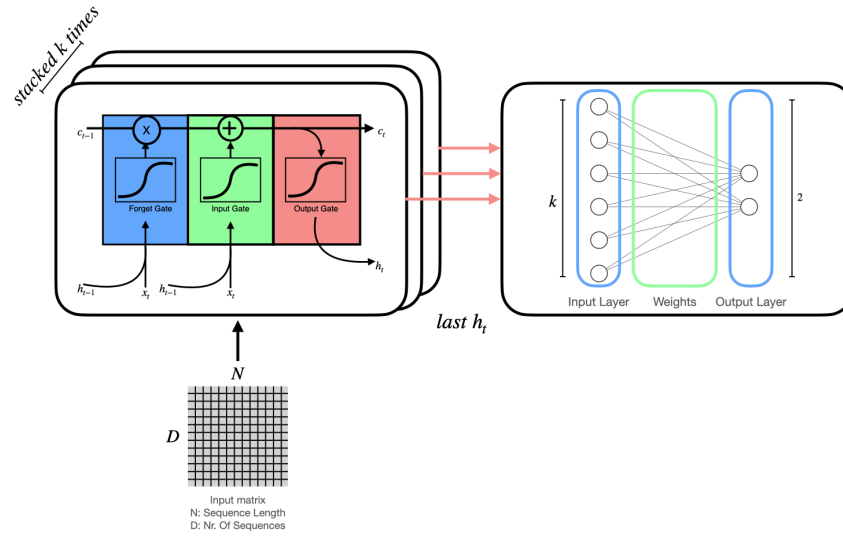
The Feedforward Neural Network was trained to minimize the weighted cross-entropy loss, using class weights computed via sklearn's [32] `compute_class_weight` function. This approach addresses class imbalance in the training data by assigning higher loss penalties to underrepresented classes. The computed class weights were passed during initialization to the PyTorch [11] `CrossEntropyLoss` function, allowing the model to pay more attention to minority class predictions.

We used the Adam [33] optimizer with a learning rate of $1e^{-4}$, as it provides adaptive learning rate updates and has been shown to work well in practice for deep learning tasks involving sparse gradients. To further improve training stability and avoid overfitting, we employed a learning rate scheduler (ReduceLROnPlateau), which reduces the learning rate by a factor of 0.5 if the validation loss does not improve for 5 consecutive epochs.

Training was performed over 100 epochs using mini-batches of 64 patterns per batch. After each epoch, the model was evaluated on the validation set to track performance metrics including accuracy, F1 score, precision, and recall. These metrics allowed us to monitor not only the raw predictive performance, but also the model's balance between false positives and false negatives, which is particularly important in the context of storm damage prediction.

This training setup was chosen to ensure stable convergence, account for class imbalance, and enable dynamic adjustment of the learning rate during training.

3.2.0.2 Long Short Term Memory Neural Network (LSTM)



3.2.1 Transformer

TBD

3.3 Software Engineering

3.3.1 Backend

3.3.1.1 Technologies

3.3.1.2 Architecture

3.3.2 Frontend

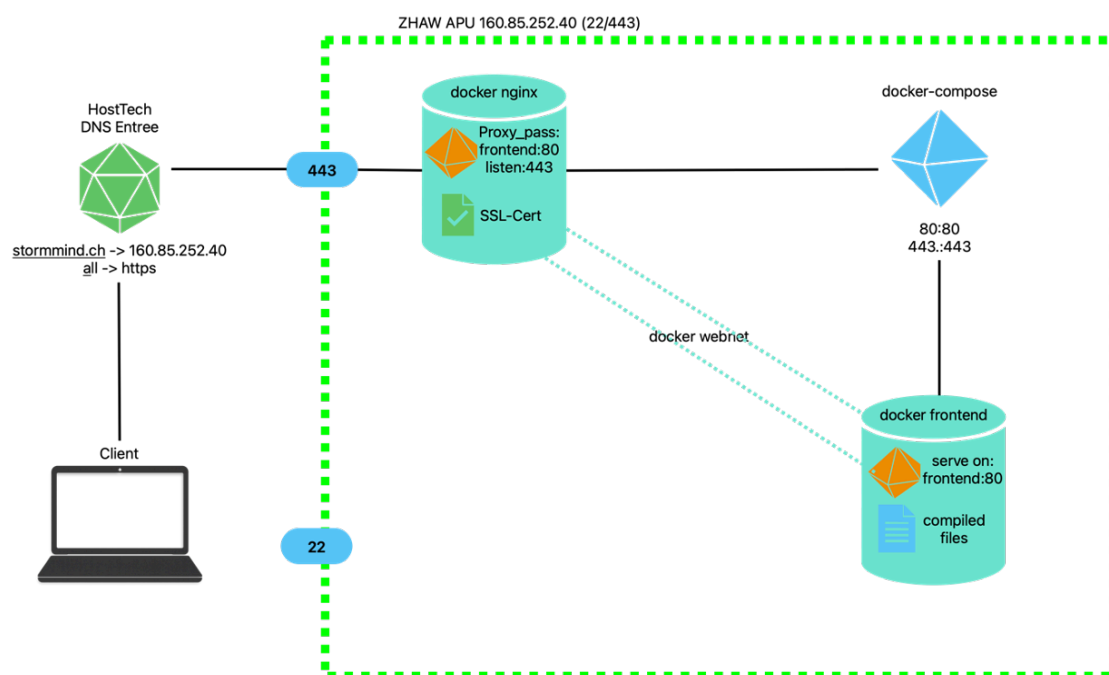


Figure 3.12 – web routing: created with apple freeform, laptop from chatgpt (prompt: erstelle mir ein png eines minimalistischen laptops ohne hintergrund)

3.3.2.1 Technologies

The Frontend consists of a react/vite repository. The DNS Entree was made on Hosttech and references an instance on the Openstack cluster of ZHAW [34]

3.3.3 Test Concept

4 Results

4.1 Results of AI Engineering

To evaluate model performance, we conducted x experiments based on the configurations detailed in Section 3.2. The first experiment, using a standard feedforward network, serves as the baseline. The setup was described in Section 3.2.0.1

INSERT COMPARISON OF ALL MODELS TABLE

4.1.1 Feedforward Neural Network: Results

The feedforward network achieved stable training behavior across 100 epochs, as shown in . Both training and validation loss converged early and remained relatively flat, suggesting a well-calibrated optimization setup. While the training loss steadily decreased, the validation loss plateaued, indicating that the model did not overfit and generalized reasonably well to unseen data.

Performance metrics such as accuracy, F1 score, precision, and recall also stabilized early during training, as shown in Figure 4.13. The final validation accuracy reached approximately 66%, with an F1 score around 0.59. This balance between precision and recall suggests that the model was able to capture patterns in both classes despite class imbalance.

The confusion matrix () further illustrates the model's performance. Class 0 (no storm damage) was predicted with high accuracy (1730 true positives vs. 492 false positives), while Class 1 (storm damage) showed moderate performance (534 true positives vs. 376 false negatives). Although the model exhibits a slight bias toward the majority class, it still correctly identifies a significant proportion of storm damage events, which is critical for real-world risk prediction.

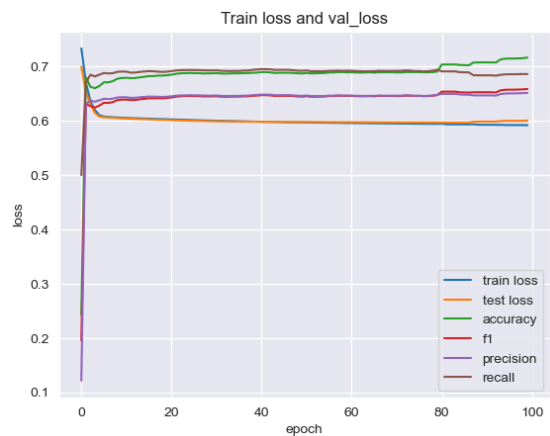


Figure 4.13 – Training of the FNN

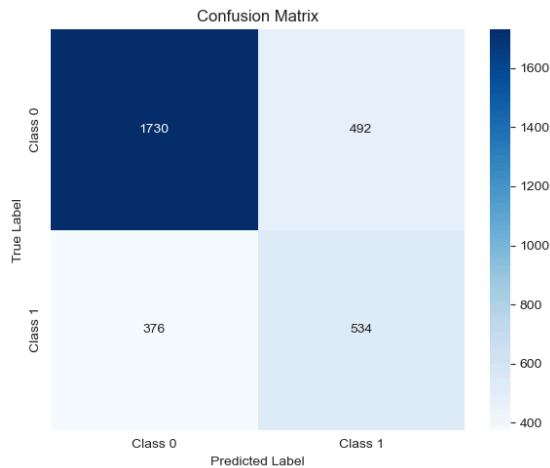


Figure 4.14 – Confusion Matrix of the FNN

Overall, the feedforward network serves as a solid baseline, offering balanced generalization and a reliable starting point for evaluating more complex architectures.

4.1.2 LSTM Neural Network

4.2 Combined

4.3 Conclusion

Table 4.2 – Results of the different experiments

Model	Accuracy	F1 Score
FNN	10014	1971 - 2002
LSTM	3132	2003 - 2013
Transformer	3132	2013 - 2023

4.4 Software Results

5 Discussion and Outlook

100

- [1] S. F. R. I. WSL, *USDB_1972_2023_ohneSchadenszahlen_ohneBeschriebe*. (2023).
- [2] “Austausch zu Unwetterschäden und Daten.” [Online]. Available: https://teams.microsoft.com/l/meetup-join/19%3ameeting_ZDk5ODM1MWQtN2E2Yi00NDZjLWFiNTEtOWE0ZWU4ODQ3YzA1%40thread.v2/0?context=%7b%22Tid%22%3a%225d1a9f9d-201f-4a10-b983-451cf65cbc1e%22%2c%22Oid%22%3a%225f85a69b-df7a-4a9a-acab-f5ad7d25b1a9%22%7d
- [3] “Erdrutsch.” Jan. 13, 2025. Accessed: May 04, 2025. [Online]. Available: <https://de.wikipedia.org/w/index.php?title=Erdrutsch&oldid=252204629>
- [4] Maria, “Gewicht nasser Erde: Formel zum Umrechnen.” Accessed: May 06, 2025. [Online]. Available: <https://hortica.de/gewicht-nasse-erde/>
- [5] Designerpart, “Schüttgut-Gewicht - Big Bag Puhm | Alles über Gewicht und Volumen.” Accessed: May 06, 2025. [Online]. Available: <https://bigbag-puhm.at/handhabung/schuettgut-gewicht/>
- [6] “NN SVG.” Accessed: May 03, 2025. [Online]. Available: <http://alexlenail.me/NN-SVG/>
- [7] C. C. Aggarwal, *Neural Networks and Deep Learning: A Textbook*. Cham: Springer International Publishing, 2023. doi: 10.1007/978-3-031-29642-0.
- [8] I. Mrázová, “Multi-Layered Neural Networks.”
- [9] F.-P. Schilling and Z. Cai, “Lecture 05: Sequential Models,” Mar. 19, 2025.
- [10] S. Hochreiter and J. Schmidhuber, “Long Short-Term Memory,” *Neural Computation*, vol. 9, no. 8, pp. 1735–1780, Nov. 1997, doi: 10.1162/neco.1997.9.8.1735.
- [11] “PyTorch Foundation.” Accessed: May 06, 2025. [Online]. Available: <https://pytorch.org/>

- [12] D. Thakur, "LSTM and Its Equations." Accessed: May 05, 2025. [Online]. Available: <https://medium.com/@divyanshu132/lstm-and-its-equations-5ee9246d04af>^o
- [13] A. Vaswani *et al.*, "Attention Is All You Need." Accessed: May 26, 2025. [Online]. Available: <http://arxiv.org/abs/1706.03762>^o
- [14] Q. Wen *et al.*, "Transformers in Time Series: A Survey." Accessed: May 26, 2025. [Online]. Available: <http://arxiv.org/abs/2202.07125>^o
- [15] S. J. D. Prince, "Understanding Deep Learning."
- [16] S. Frank-Peter, "09_Transformers," Apr. 16, 2025.
- [17] P. Zippenfenig, "Open-Meteo.Com Weather API." [Online]. Available: <https://open-meteo.com/>^o
- [18] "OpenCage - Easy, Open, Worldwide, Affordable Geocoding and Geosearch." Accessed: May 06, 2025. [Online]. Available: <https://opencagedata.com/>^o
- [19] K. Liechti, "RE: Anfrage Zur Nutzung Der Unwetterschadens-Datenbank Für Bachelorarbeit." Nov. 29, 2024.
- [20] "MeteoSwiss IDAWEB: Login at IDAWEB." Accessed: May 06, 2025. [Online]. Available: <https://gate.meteoswiss.ch/idaweb/login.do>^o
- [21] P. Zippenfenig, "Professional API Key for Research Purposes."
- [22] "Maps of Switzerland - Swiss Confederation - Map.Geo.Admin.Ch." Accessed: May 06, 2025. [Online]. Available: https://map.geo.admin.ch/#/?map?lang=en¢er=2660000,1190000&z=1&topic=ech&layers=ch.swisstopo.zeitreihen@year=1864,f;ch.bfs.gebaeude_wohnungs_register,f;ch.bav.haltestellen-oev,f;ch.swisstopo.swisstlm3d-wanderwege,f;ch.vbs.schiessanzeigen,f;ch.astra.wanderland-sperrungen_umleitungen,f&bgLayer=ch.swisstopo.pixelkarte-farbe^o
- [23] "GIS-Browser Geoportal Kanton Zürich." Accessed: May 06, 2025. [Online]. Available: <https://geo.zh.ch/maps?x=2693065&y=1253028&scale=279770&basemap=arelkbackgroundzh>^o
- [24] "Vergraben und vergessen." Accessed: May 06, 2025. [Online]. Available: <https://www.derbund.ch/vergraben-und-vergessen-413137488243>^o
- [25] "Phone call Hochbau und Umwelt Affoltern am Albis." Aug. 04, 2025.
- [26] "phone call Hochbau Amt Zürich." Aug. 04, 2025.
- [27] "phone call Amt für Raum Entwicklung und Vermessung." Aug. 04, 2025.
- [28] D. Ueltschi, "Bodenbeschaffenheitskarte."

- [29] F. GIS, “[ARE-JIRA] GIS-2262 [EXTERN] Bodenbeschaffenheitskarte.”
- [30] *Amtliches Gemeindeverzeichnis der Schweiz - MS-Excel Version*, no. 286080. Bundesamt für Statistik (BFS) / BFS. Accessed: Feb. 25, 2025. [Online]. Available: <https://dam-api.bfs.admin.ch/hub/api/dam/assets/286080/master>[◦]
- [31] “2.3. Clustering.” Accessed: May 13, 2025. [Online]. Available: <https://scikit-learn/stable/modules/clustering.html>[◦]
- [32] “Scikit-Learn: Machine Learning in Python — Scikit-Learn 1.6.1 Documentation.” Accessed: May 06, 2025. [Online]. Available: <https://scikit-learn.org/stable/#>[◦]
- [33] D. P. Kingma and J. Ba, “Adam: A Method for Stochastic Optimization.” Accessed: May 06, 2025. [Online]. Available: <http://arxiv.org/abs/1412.6980>[◦]
- [34] “Login - OpenStack Dashboard.” Accessed: May 06, 2025. [Online]. Available: <https://apu.cloudlab.zhaw.ch/auth/login/?next=/>[◦]
- [35] S. F. R. I. WSL, “Infos_Daten_Unwetterschadensdatenbank_WSL_english.” 2023.

List of Figures

Figure 2.1	Illustration of a Neural Network with 3 layers. Illustrated with [6]	5
Figure 2.2	Training Procedure of the backpropagation algorithm	6
Figure 2.3	RNN	8
Figure 2.4	4 times unrolled RNN	8
Figure 2.5	Schematic illustration of an LSTM cell highlighting the internal gating structure. The colored blocks represent the three core gates—Forget (blue), Input (green), and Output (red)—and show how they interact with the cell and hidden states to regulate information flow.	9
Figure 2.6	Self-attention mechanism illustrated with matrices. All matrices have shape $D \cdot N$, where D is the sequence length and N is the feature dimension. The input matrix is projected into three separate matrices: Queries (Q), Keys (K), and Values (V). The attention weights are computed by multiplying Q with the transpose of K , followed by the Softmax function. The result is then used to weight the V matrix, producing the final output as $\text{Softmax}(QK^T) \cdot V$. [15]	11
Figure 2.7	Abstracted illustration of the encoder–decoder architecture. The encoder receives an input sequence x_1, \dots, x_n and transforms it into a sequence of contextualized representations, here called the Encoder Vector, which is symbolically represented by two arrows to emphasize its role in guiding the decoding process. The encoder vector are passed to the decoder, which generates an output sequence y_1, \dots, y_k , where the output length k may differ from the input length n . [7]	12
Figure 3.8	Example clustering of all Swiss municipalities with $k = 6$	17
Figure 3.9	Training Pipeline illustrated	19
Figure 3.10	Illustration of the used FNN	20
Figure 3.11	21
Figure 3.12	web routing: created with apple freeform, laptop from chatgpt (prompt: erstelle mir ein png eines minimalistischen laptops ohne hintergrund)	

..... 22

Figure 4.13 Training of the **FNN** 24

Figure 4.14 Confusion Matrix of the **FNN** 24



List of Tables

Table 3.1	Datasets splits	19
Table 4.2	Results of the different experiments	24

A Appendix

AA Disclaimer

“Information on the Data of the Swiss flood and landslide damage database managed by WSL

Please note the following when using the data:

- Names of municipalities refer to the state of 1996. I.e. some municipalities have merged.
- Media reports are the main source of information. There are local and regional differences in reporting. In addition, the focus of the media has changed over time.
- In some cases, it is difficult to assign the damage to a location and / or municipality (in a few cases of doubt, the damage is assigned to the respective canton capital or even the Swiss capital)
- The coordinates have been set based on information from media reports, images, etc. They can therefore deviate greatly from the real main point of damage.

The following must be observed when publishing:

- If the data values are cited or published, they must be provided with at least a reference to the source (“WSL Swiss Flood and Landslide Damage Database”).
- It must be clearly mentioned that the damage data are only estimates.
- Damage values must always be rounded in publications.
- No monetary damage may be published at community level, but only in aggregated form (regions, cantons).
- Monetary damage may only be published in a form that does not allow any conclusions to be drawn about individuals and individual objects.“[35]

AB Original Data Features

Gemeinde, Gemeindenummer, Weitere Gemeinde, Kanton, Prozessraum, MAXO Datum, Datum, MAXO Zeit, Zeit, Gewässer, Weitere Gewässer, Hauptprozess, Hauptprozess Rutschung Unterteilung, Hauptprozess Wasser/Murgang Unterteilung, Weitere Prozesse, Schadensausmass: gering [0.01-0.4]; mittel [0.4-2]; gross/katastrophal[>2] oder Todesfall [Mio. CHF], x-Koordinate, y-Koordinate, Schadenszentrum; Gemeindegebiet falls nicht bekannt, Grossereignisnummer; mehrere Ereignisse; welche aufgrund meteorologischer oder räumlicher Gegebenheiten zusammengefasst werden, Gewitterdauer MAXO, Gewitterdauer [Std.], Gewitter Niederschlagsmenge MAXO, Gewitter Niederschlagsmenge [mm], Dauerregen Dauer MAXO, Dauerregen Dauer [Std.], Dauerregen Niederschlagsmenge MAXO, Dauerregen Niederschlagsmenge [mm], Schneeschmelze MAXO, Schneeschmelze, Ursache nicht bestimmbar MAXO, Ursache nicht bestimmbar, ID

